

Geodetic measurement of deformation in the Ventura basin region, southern California

Andrea Donnellan*

*Jet Propulsion Laboratory
California Institute of Technology
Pasadena, CA 91109*

Bradford H. Hager

Robert W. King

Thomas A. Herring

*Department of Earth, Atmospheric and Planetary Sciences
Massachusetts Institute of Technology, Cambridge, MA 02199*

Journal of Geophysical Research

Submitted April 16, 1993

Revised September 9, 1993

*Formerly at: NASA Goddard Space Flight Center Greenbelt, MD 20771

ABSTRACT

We have measured the deformation in the Ventura basin region, southern California, with Global Positioning System (GPS) measurements carried out over 4.6 years between 1987 and 1992. The deformation within our network is spatially variable on scales of tens of kilometers, with strain rates reaching $0.6 \pm 1 \mu\text{rad/yr}$ in the east-central basin. Block-like rotations are observed south and northwest of the basin where the maximum shear strain rates are an order of magnitude lower ($0.06 \pm 1 \mu\text{rad/yr}$ to the south). We also observed clockwise rotations of $1\text{--}7^\circ/\text{Myr}$. Shear strain rates determined by comparing angle changes from historical triangulation spanning several decades and GPS measurements give consistent, though less precise results. The geodetic rates of shortening across the basin and Western **Transverse** Ranges are lower than those estimated from geological observations, but the patterns of deformation from the two methods agree qualitatively.

INTRODUCTION

The Ventura basin is an east-west trending sedimentary basin located in the Western Transverse Ranges province of southern California, approximately 60 km northwest of Los Angeles (Figure 1). The basin is about 10-15 km wide and stretches for 100 km from the Santa Barbara Channel eastward to the western edge of the San Gabriel Mountains. Thrust faults that dip away from the basin bound the northern and southern margins (Figure 2). The basin itself is a synclinal structure with an extraordinarily thick sedimentary section estimated to be 14-17 km deep [Norris and Webb, 1990; Luyendyk and Hornafius, 1987]. The geologic record implies rapid convergence across the central basin, with shortening rates on the order of 25 ± 5 mm/yr estimated for the last 250 ± 50 ka [Yeats, 1983, Huftile and Yeats, 1992]. Seismological, gravity, and heat flow observations also indicate that the basin is tectonically active.

In this study we present the results of a geodetic experiment designed to test whether the rates and spatial distribution of deformation measured with space geodesy are compatible with the estimated geologic rates. Over a period of 4.6 years, we collected four epochs of GPS measurements from a network that spans the Ventura basin and have included data from other experiments as well (Table 1) [Feigl et al., 1993]. We have estimated the velocities with uncertainties less than 2-3 mm/yr at 95% confidence for most stations in the vicinity of the Ventura basin. In addition, we used historical triangulation measurements to obtain an estimate of the strain field over a 28-75 year time period to compare the rates estimated from the two techniques.

Geologic Background

The Ventura basin originated as a **forearc** basin some 400 km south of its present location [Crowell, 1987]. Subduction of the East Pacific Rise during the late Cretaceous and early Tertiary created a foredeep basin in which the first sediments were deposited into what are now the San **Joaquin**, Los Angeles, and Ventura basins. In the early Miocene (22 Myr), **crustal** stretching replaced subduction, forming the individual basins. At around 6 Myr rapid subsidence was renewed and the surface of the Ventura basin may have reached 1.5 km below sea level, providing a deep depository for great thicknesses of Pliocene sediments. The current compressive regime began during the middle Pleistocene **as** the area experienced uplift, folding, and faulting [Norris and Webb, 1990].

East-west trending compressive structures characterize the present-day Ventura basin. Yeats [1983] and Çemen [1989] divide the basin into three parts: offshore, central, and eastern. Although we maintain their divisions, we further subdivide the basin in terms of the morphology and deformation rates inferred from the geologic record. The central basin, encompassing the area surrounding the town of Ventura, is broad. It is bounded on the north by the Red Mountain thrust fault and on the south by the Oxnard Plain. The **east-central** Ventura basin, which lies in the Fillmore/Santa Paula area, is narrower. The center trough of the east-central basin is a **synclinal** structure, bounded on the north by the San Cayetano thrust fault and on the south by Oak ridge, an **anticlinal** structure overlying the Oak Ridge fault. The thrust faults dip away from the east-central and central basin. The San **Cayetano** fault and the Oak Ridge fault pinch the basin and are less than 3 km apart at their closest point, just east of the town of Fillmore, where they terminate in a **synclinal** structure [Çemen, 1989]. The eastern Ventura basin is broader and is bounded on the south by the Santa Susana fault, a north-dipping thrust fault that outcrops on the southern margin

of Oak ridge [Reed *and Hollister, 1936*]. It begins its exposure where the San Cayetano and Oak Ridge faults die out. Folds with east-west trending axes are found on either side of the basin. We will sometimes refer to the offshore Ventura basin, west of the central basin, as the Santa Barbara Channel.

Estimates of rates of north-south convergence across the basin in excess of 20 mm/yr [e.g. *Yeats, 1983; Rockwell, 1988; Çemen, 1989*] depend on inferences of both ages of deformation and geometries of geologic structures. *Molnar* [1993] argues that the ages of the formations used to determine the geologic convergence rates have been underestimated by up to a factor of two, but that the amounts of shortening are well constrained. The dates are sometimes obtained from the same formations located elsewhere, tens of kilometers away, and therefore may not apply. This could reduce the convergence rate and bring it closer to *Yeats'* [1983] lower bound of 12 mm/yr of shortening for the east-central basin. The high rates are also based on surface slip rates of the faults that bound the basin. In the analyses it is assumed that the thrust faults flatten at depth into *décollements*. If, instead, the faults maintain the same dip at depth as at the surface, the horizontal convergence would be 5-10 mm/yr [*Yeats and Huftile, 1992*].

The rate of shortening across the Ventura basin over the last 200 ka is comparable to the total shortening rate across the Western Transverse Ranges during the last 3–5 million years. *Namson and Davis [1988]* have estimated a geologic rate of convergence of 17-26 mm/yr along a north-south cross-section of the Western Transverse Ranges, *Molnar* [1993] estimates that the rate is closer to 10 mm/yr, similar to his estimate for the Ventura basin. It is plausible that all or most of the recent deformation of the Western Transverse Ranges is being accommodated across the Ventura basin.

Geophysical Observations

In the east-central Ventura basin earthquakes occur to depths of 28 km, nearly twice the maximum depth observed over most of southern California [Bryant and Jones, 1992]. The deep earthquakes are confined to a localized zone and are interpreted to be due to rapid shortening and subsidence of the basin. In the same region, the lowest heat flow values in southern California are observed [De Rito et al., 1989] (48 mW/m² versus typical values of 70 mW/m² elsewhere). The most pronounced negative isostatic gravity anomalies in southern California (up to -60 regal) are also found in the Ventura basin [Roberts et al., 1981]. Anomalies in other basins, such as the Santa Maria and Los Angeles basins, range from -25 to -35 regal.

The rapid rate of deformation implies high uplift rates of the adjacent ranges and rapid rates of sedimentation. This is in agreement with gravity anomalies, which indicate that the basin is filled with sediments to depths up to 14 km [Luyendyk and Hornafius, 1987]. Sedimentation and subsidence depress the temperature profile; the low heat flow indicates that the basin is colder, and presumably more brittle, to greater depths than the surrounding region, providing an explanation for why earthquakes occur deeper there than elsewhere [Bryant and Jones, 1992].

Paleomagnetic observations have been used to show that clockwise rotations on the order of 5°/Myr have occurred on geologic time-scales in the Western Transverse Ranges [Hornafius, 1985; Kamerling and Luyendyk, 1985]. Rotations of 15 °/Myr have been estimated for the eastern Ventura basin [Levi et al, 1986]. Jackson and Molnar [1990] show that slip vectors from major earthquakes in this region and observations from VLB1 measurements are consistent with continuing clockwise block rotations.

Geodetic Background

Recent geodetic studies indicate that a zone of active convergence runs along the southern portion of the Transverse Ranges. In the Santa Maria fold and thrust belt at the western edge of the Transverse Ranges, crustal shortening is occurring at a rate of $2 \pm 1 \text{ mm/yr}$ and is coupled with $3 \pm 1 \text{ mm/yr}$ of right-lateral shear [Feigl et al., 1993]. The zone of shortening steps southeastward and the rate increases to $6 \pm 2 \text{ mm/yr}$ in the Santa Barbara Channel [Larson and Webb, 1992; Larsen et al., 1993; Feigl et al., 1993]. Further east, negligible deformation is observed to the south of the Ventura basin [Webb, 1991], while about $3 \pm 1 \text{ mm/yr}$ of contraction are observed to the north between the basin and the San Andreas fault [Eberhart-Phillips et al., 1990]. The zone of contraction can also be found east of the Ventura basin along the southern margin of the San Gabriel Mountains. About $4 \pm 1 \text{ mm/yr}$ of shortening are measured between the San Gabriel Mountains and the Pales Verdes Peninsula (site PVER in this study) [Feigl et al., 1993].

North of the San Gabriel Mountains, shear is occurring parallel to the San Andreas fault at a rate of $0.30 \pm 0.03 \text{ } \mu\text{strain/yr}$ [Cline et al., 1984], and $0.38 \pm 0.02 \text{ } \mu\text{strain/yr}$ is estimated across the fault north of the Ventura basin [Eberhart-Phillips et al., 1990]. Away from the fault both Eberhart-Phillips et al. and Cline et al. find that the shear strain is lower and is oriented in the direction of the Pacific plate motion.

OBSERVATIONS AND ANALYSIS

We designed our original 1987 GPS network to measure the shortening across the geologically most active part of the Ventura basin and later included additional sites to measure deformation surrounding the basin. We selected triangulation monuments for the original network to estimate the deformation after the first epoch of GPS measurements. This limited our choice

of stations because many of the original horizontal control marks were destroyed, but the network provided good coverage of the central and east-central part of the basin. (In some cases our stations occupy marks near the original monument and we rely on geodetic ties to recover the historical triangular ion,) We could not always occupy all sites simultaneously, so we collected data at Pales Verdes (PVER) during every session to provide a common reference (Table 1). We observed over a period of 2–5 days, for 8-hour sessions during the first three experiments and for 20-hour sessions during the 1992 experiment.

Data Analysis

We performed the analysis in two steps. We first analyzed each day of data separately using the GAMIT software developed at the Massachusetts Institute of Technology (MIT) and Scripps Institution of Oceanography [King and Bock, 1993]. To improve the estimates of the satellite orbital parameters, and hence of site coordinates, we included in our analysis data from a global network of GPS tracking stations, constraining their positions to values determined from an analysis of GPS and VLBI between 1984 and 1992 [Feigl et al., 1993]. We also used well-known techniques to resolve the integer-cycle ambiguities in the doubly difference phase measurements [Schaffrin and Bock, 1988; Dong and Bock, 1989; Feigl et al., 1993].

In the second step we combined the individual experiments with VLBI and other GPS data to obtain estimates of site velocities using the GLOBK software package developed at the Harvard Smithsonian Center for Astrophysics and MIT [Herring, 1993], GLOBK combines the adjustments of the site-coordinate and orbital parameters and their covariance matrices from the individual-day solutions using a Kalman filter, thus allowing stochastic constraints to be placed on the variation of orbital parameters from day to day [Herring et al.,

1990; *Herring et al.*, 1991]. The Ventura basin data were analyzed in combination with a larger set of GPS and VLBI data collected in California and globally between 1984 and 1992 [*Feigl et al.*, 1993]. This global analysis strengthens our results by constraining coordinates of the global sites used to determine the satellites' orbits and the regional sites used to define the reference frame for our Ventura basin network,

The 1σ uncertainties from the global analysis for both the north and east components of velocities are less than 2 mm/yr (Table 2, Figure 3) for all sites except for Santa Clara (SCLA) and Cuyama 2 (YAM2), which have fewer high-quality observations and shorter time spans between the first and last observations. These uncertainties were obtained by scaling the formal errors from the global analysis by a factor determined from comparisons between VLBI and GPS estimates and the long-term scatter of the GPS results for all of California [*Feigl et al.*, 1993]. With this scale factor applied, chi-square per degree of freedom, χ^2/ν , for the global solution is 1.2, and for the Ventura basin experiments alone, 1.7. Examination of the long-term repeatabilities for each of the sites (Figure 4) suggests that most of the scatter is due to outliers associated with the 1990 experiments, which featured a particularly weak fiducial network. The evidence for this inference is strongest for the stations with four or more observations (CATO, HOPP, LACU, SAFE, and SOLI), though the largest outlier occurs in the north component of YAM2. Since 1990 falls near the middle of the span of measurements, an outlier affects mostly the mean position rather than the velocity of a site. For example, deletion of the middle point in the north component of YAM2 would affect the slope of the line much less than the intercept. If we remove the 1990 experiment from the solution, χ^2/ν for the Ventura basin experiments drops to 1.0 and all of the estimated velocities agree with our original estimates within the uncertainties expected from the measurement noise. No velocity changes by more than 2 mm/yr except the east

component of Santa Paula 2 (SNP2), for which the 1987 observation has a large uncertainty.

GPS Results

We used the GPS velocities weighted by their uncertainties to estimate the **two-dimensional** velocity gradient tensor and related parameters such as the strain, dilatation, and rotation rates for subregions of the network (Figure 5, Tables 2 and 3). The symmetric part of this tensor is the strain rate tensor, while the **antisymmetric** part gives the rotation rate. We used weighted least squares to solve the following two systems of equations for the components (\dot{u}_{ii}) of the velocity gradient tensor.

$$\dot{u}_e = \dot{u}_{ee}E + \dot{u}_{en}N \quad (1)$$

$$U''_n = \dot{u}_{ne}E + \dot{u}_{nn}N \quad (2)$$

where \dot{u}_e and \dot{u}_n are the east and north components of the velocity of a station. E and N refer to the east and north baseline components respectively. From the velocity gradient tensor we calculated the following **crustal** deformation parameters [Drew and Snay, 1989]:

$$\text{areal dilation rate, } A = \dot{u}_{nn} + \dot{u}_{ee} \quad (3)$$

$$\text{clockwise rotation rate, } w = \frac{(\dot{u}_{en} - \dot{u}_{ne})}{2} \quad (4)$$

$$\text{horizontal shear rate on NE \& NW striking planes, } \dot{\gamma}_1 = \dot{u}_{ee} - \dot{u}_{nn} \quad (5)$$

$$\text{horizontal shear rate on N \& E striking planes, } \dot{\gamma}_2 = \dot{u}_{en} + \dot{u}_{ne} \quad (6)$$

$$\text{maximum horizontal shear rate, } \dot{\gamma} = \sqrt{(\dot{\gamma}_1^2 + \dot{\gamma}_2^2)} \quad (7)$$

$$\text{azimuth of maximum contraction, } \theta = \frac{\arctan(\frac{-\dot{\gamma}_2}{\dot{\gamma}_1})}{2} \quad (8)$$

For calculating the velocity gradients we divided the basin into regions containing 3-5 sites that best represented the tectonic characteristics (Figure 5). Although we prefer to use

at least four sites so that the solution is **overdetermined**, there is so much spatial variability of strain within the network that in one case we use only three sites. We do not show results for the region due north of the basin because the short time-span between observations at MPNS makes them less reliable. Instead, we use the strain rate from *Eberhart-Phillips et al. [1990]*; our results **are** consistent with these, but less precise,

Comparison with Triangulation Data

First-order triangulation observations were performed in the southern subnetwork **as** early as 1898, in the eastern subnetwork in the 1930's, 1950's, and 1960's, and in the east-central subnet work in 1959 and 1975 (Figure 6). Although the precision of these observations (**0.6''–1.4''**, or 0.3-0.6 μrad) is much lower than for GPS, the long time-span offers the opportunity to obtain independent estimates of strain rates for some parts of the basin. Because the triangulation alone was insufficient to resolve the strain rate for the eastern and east-central subnetworks, we included angles computed from a single epoch of GPS observations for these subnetworks.

Using a modification of *Frank's [1966]* method similar to that used by *Prescott [1976]*, we calculated the first and second components of shear strain rate, **as well as** the maximum shear strain rate and azimuth of maximum compression, from the angle changes. We solve the equation

$$\phi_{ij} = t_j(A_i^1\dot{\gamma}_1 + A_i^2\dot{\gamma}_2) + \phi_i^0$$

where ϕ_{ij} is the observed angle at t_j , the time of the j^{th} survey, and A_i^1 and A_i^2 depend on the orientation of the i^{th} angle. Because the errors from GPS are considerably smaller than those of triangulation, we weighted the calculation by the errors and solved for $\dot{\gamma}_1$, $\dot{\gamma}_2$ and ϕ_i^0 .

We were not able to occupy the same monuments that were used during the triangulation surveys for the sites Castro Peak (CATO) and San Fernando (SAFE). For Castro, the triangulation history is sufficient to estimate strain rates without including the angles from GPS. For San Fernando, we relied on ties to nearby monuments SAF8 and SAF3 (stamped San Fernando 1898 and San Fernando 1898 RM 3 respectively, but now destroyed) to compare the GPS angles to the original angles measured near SAFE. We corrected all of the triangulation angles for the deflection of the vertical, which was as high as 1.4", but more typically 0.5" [Donnellan, 1991].

With one exception, the triangulation and GPS estimates are consistent within their combined uncertainties (Table 4). Most significantly, the triangulation results confirm the large (0.3-0.6 $\mu\text{rad}/\text{yr}$) strain rate in the east and east-central basin. The only parameter for which the triangulation and GPS estimates differ significantly is $\dot{\gamma}_2$ for the east-central subnetwork. The predicted angle changes (dashed line, Figures 6a-c) from the GPS-only strain rates differ considerably from those obtained for the triangulation (plus one epoch of GPS) in the east-central basin (solid line, Figure 6a). (The predicted angle changes are determined by adjustment of the entire network, not each angle separately, so the model lines do not in general fit individual angle changes.) There is little redundancy in the triangulation data for this subnetwork, however, and the triangulation results could be made to agree with the GPS by the removal of one or two observations from the 1959 survey (Figure 6a). In contrast, the eastern and southern networks show similar scatter for the GPS- and triangulation-predicted angle changes (Table 4, Figures 6b-c). The agreement between the GPS and triangulation inferred strain rates improves and wrms scatter is reduced with increased numbers of observations (Table 4). For the eastern subnetwork the uncertainties in strain rate parameters are comparable to those from the GPS analysis, but for the southern

and east-central networks, they are typically two to three times larger. The *a posteriori* standard deviation of unit weight was near unity for each of the three subnetworks, so it was unnecessary to scale the estimated uncertainties.

DISCUSSION

The observed motions are due primarily to tectonic causes and are not likely due to either site instabilities or fluid withdrawal. All of our monuments are first order and have been carefully examined for site stability. We can account for about 0.2 mm/yr of horizontal motion attributable to fluid withdrawal by assuming an elastic model, and using the depth and production of the most prolific oil field in the basin [Donnellan, 1991]. Oil production of the Ventura basin has dropped off considerably in the last few decades [D.C. Cavit, Unocal, written communication; Cal. Div. of Oil and Gas, 1989]. Models of large earthquakes that occurred nearby also show that displacements from the earthquakes had little effect on sites in the Ventura basin network [Donnellan, 1991].

The east-central basin is the most rapidly deforming region, with a maximum shear strain rate nearly twice as large as that measured across the San Andreas fault. We observe north-south compression across the basin in a zone about 15 km wide and at least 40 km long, with right-lateral shear superimposed over the entire network. Block-like motion is occurring south of the basin and in the Western Transverse Ranges to the north of the Santa Barbara Channel, and intermediate strain rates are observed in the other subregions. Only across the basin do we observe any substantial dilatation, where lines are shortening at about 7 mm/yr. Clockwise rotations of up to 7°/Myr are pervasive. The triangulation observations, although noisy, are consistent with these rates having been sustained for at least 30-50 years across the basin and for 90 years south of the basin,

The azimuth of maximum contraction is oriented perpendicular to the trend of the **basin** in both the eastern and east-central sub-regions. The velocities of sites relative to Santa Paula (SNPA) on the south side of the basin increase to the west, while the velocities on the northern side may increase, though less strongly, to the east. It appears that in the eastern basin the north side has overridden the south side. This is apparent in the geology and in the southern motion of San Fernando (SAFE) relative to the basin and is consistent with a south verging thrust fault (Santa Susana fault) that may be an extension of the San **Cayetano** fault system. Unlike the central and east-central basin, the eastern basin is bounded on the south by a north-dipping thrust fault with no recognized fault bordering the north. The Oak Ridge and San **Cayetano** faults pinch together and die out in the eastern basin.

The maximum shear strain rate drops off by about a factor of two east of the narrow east-central Ventura basin. There is an intermediate amount of **strain** occurring in the central basin. Although the data are limited, there is a suggestion that the strain rate in the central basin is higher ($\dot{\gamma} = 0.5 \pm 0.1 \mu\text{strain/yr}$) if the site **Cotar** (COTR) is not included in the calculation. With COTR removed the dilatation in the central basin is comparable to the east-central basin. It appears that the entire Ventura basin is undergoing north-south contraction, while little deformation is occurring in the rest of the network except for the northern region, in which shearing is the primary mode of deformation and $\dot{\gamma} = 0.3 \pm 0.1 \mu\text{rad/yr}$. The northwest region appears to be a transition zone between the rapidly contracting basin and the mountains to the west-northwest (far-western region), which show almost negligible deformation. This suggests that essentially all of the **north-south** contraction of the section of the Western Transverse Ranges that includes the Santa Barbara Channel is being accommodated across the Channel, along the extension of the Ventura basin. Geodetic measurements show that the eastern Channel is shortening at a

rate of 6 ± 2 mm/yr [Larson and Webb, 1992; Larsen *et al.*, 1993; Feigl *et al.*, 1993], similar to that of the basin.

The southern region exhibits little deformation and is block-like in nature. We observe a small amount of shearing that is sub-parallel to the Pacific-North American plate motion. The deformation accounts for about 2-3 mm/yr of right-lateral shear across a region several times larger than the basin. Most of the motion is attributable to rotation and accounts for 4-5 mm/yr of variation in relative velocity across the subnetwork.

We estimated how much of this shear is associated with the San **Andreas** fault and other nearby faults by using locking depths and slip rates previously estimated from geodetic measurements. We used the fault displacement model of *Eberhart-Phillips et al. [1990]* to calculate the expected displacements in the Ventura basin due to the San **Andreas**, **Garlock**, and Big Pine faults. Slip at depth on the three faults has little effect on the Ventura basin network (Figures 3 and 7). The largest, though still minor, effects are at Mount **Piños** (**MPNS**) and Yam 2 (**YAM2**), which are nearest to the San **Andreas** fault. Even for those sites, however, the motion is barely outside the standard deviation of the observed motion.

Our results suggest that the deformation is quite variable spatially. Within this network the geodetic results cannot be fit by the broad simple shear zone that has been applied to California [*Ward*, 1988]. The regional compression that we observe may result from convergence actively driven by a small-scale thermal convection cell in the upper mantle beneath the Transverse Ranges [*Humphreys and Hager*, 1990]. *Sheffels and McNutt [1986]* propose that the Ventura basin, within the Western Transverse Ranges, marks a boundary in which a thin southern plate is subducting under a thick northern plate.

The short-term rate of deformation that we have measured is about half of the generally accepted long-term geologic shortening rate of the both the Ventura basin and the Western

Transverse Ranges [Yeats, 1983, Rockwell, 1988, Çemen, 1989; Namson and Davis, 1988]. The geologic record reflects the average rate of deformation over many earthquake cycles, or cycles of elastic strain accumulation and release. At the time of an earthquake, rapid deformation occurs in a very narrow zone, During the interseismic phase deformation should occur in a much broader zone. We observe an average of 7 ± 2 mm/yr of contraction between the San Andreas fault and the coast to the south. Regionally, over a zone that extends for 60km both north and south of our network, the north-south contractions 11 ± 3 mm/yr [Feigl et al, 1993], indicating either that the 17-26 mm/yr estimate of convergence given by Namson and Davis [1988] is too high, or that the more recent convergence is lower than the 5 Myr average.

An examination of the geologic data suggests that the dates used to infer the rates across the basin may be older than assumed. Huftile and Yeats [manuscript submitted to JGR] estimate a shortening rate of 6 ± 5 mm/yr during $975-250 \pm 50$ ka and a rate of 27 ± 11 mm/yr from 250 ± 50 ka to the present in the central Ventura basin. If the rate of shortening has actually been constant over the last 975 kyr then the shortening rate is 11 ± 5 mm/yr and the top of the Saugus formation (estimated at 250 ± 50 ka) is much older than expected. It is possible that the age of the Saugus formation has been underestimated [Yeats, written communication].

The high short-term rate of deformation within the basin might also be indicative of anelastic behavior. The many east-west trending folds of the basin suggest that aseismic deformation is occurring to some extent. Faults bounding the basin do show evidence for previous earthquakes, however, indicating that elastic strain accumulation and release is an important mode of long-term deformation of the basin. Scarps along the San Cayetano fault and the lack of evidence of recent creep indicate that the fault is locked between earthquakes,

which occur every 200–600 years [Rockwell, 1988]. We are able to fit the velocities in the east-central basin by allowing for creep at depths greater than ~ 5 km on the faults that bound the basin [Donnellan et al., 1993, submitted]. Because the faults in our models are locked at the surface it is possible for ground-rupturing earthquakes to occur.

We have also measured clockwise rotations of $4\text{--}7^\circ/\text{Myr}$ for most regions of the network. These rotations are comparable to paleomagnetic results, which show block rotations near the basin at rates on the order of $5^\circ/\text{Myr}$ [Hornafius, 1985; Kamerling and Luyendyk, 1985], and within the basin at rates in excess of $10^\circ/\text{Myr}$ [Levi et al., 1986].

CONCLUSIONS

Our geodetic network occupies a region only $80 \times 100 \text{ km}^2$, yet within it we have identified many different tectonic regimes. The Ventura basin itself is rapidly contracting, while the regions to the north and northwest undergo predominately shear deformation. We have observed block-like motions south of the basin and in the far-western region of our network. The geodetic results indicate that the east-central basin is deforming the most rapidly. Other observations support this conclusion. The low heat flow, deep seismicity and large gravity anomalies indicate extensive subsidence and imply rapid deformation locally in this portion of the basin. The rotation rates that we measure within the network are comparable to those inferred from paleomagnetic observations.

The high strain rates across the Ventura basin are qualitatively in agreement with the geology. Apparently, most of the present day shortening of the Western Transverse Ranges is occurring across the basin and to the west in the Santa Barbara Channel. The geodetically observed rates are lower than the proposed geologic rates for the last 0.2 Myr by a factor of two, but are consistent with the average shortening rate over the last 1 Myr. Because the

far-field shortening rate is also lower than the proposed geologic rate [*Feigl et al*, 1993], it is possible that the 0.2 Myr geologic rate has been overestimated through the use of either incorrect fault geometries or incorrect dates. At present, the level of detail of our network is insufficient to distinguish between the two,

ACKNOWLEDGEMENTS

The research described in this paper was carried out under a National Research Council Post-Doctoral fellowship at the NASA Goddard Space Flight Center, at the California Institute of Technology Seismological Laboratory, the Massachusetts Institute of Technology, and the Jet Propulsion Laboratory, California Institute of Technology, under contracts with the National Aeronautics and Space Administration (grants NAG5-1 132, NAG5-842 and NAG5-737), the U. S. Geological Survey (grant 1434-92-G-2185) and the National Science Foundation (grants EAR-8618542 and EAR-8618513). We thank the numerous people who assisted with the GPS field observations. The Ohio State University, Scripps Institution of Oceanography, the Jet Propulsion Laboratory and the University NAVSTAR Consortium (UNAVCO) lent us receivers for the observations. We gratefully acknowledge Kurt Feigl and Danan Dong for their contributions to the processing of the GPS data.

REFERENCES

- Bryant, A. S. and L. M. Jones, Anomalous deep crustal earthquakes in the Ventura basin, southern California, *J. Geophys. Res.*, 97, 437–447, 1992.
- California Dept. of Conservation, Div. oil and gas, 75th annual report of the state oil and gas supervisor, 1989.
- Cemen, I., Near-surface expression of the eastern part of the San Cayetano fault: A potentially active thrust fault in the California Transverse Ranges, *J. Geophys. Res.*, 94, 9665–9677, 1989.
- Crowell, J. C., Late Cenozoic basins of onshore southern California: Complexity is the hallmark of their tectonic history, in *Cenozoic Basin Development of Coastal California*, edited by R. V. Ingersoll and W. G. Ernst, vol. 6, pp. 207–241. Prentice Hall, Inc., Englewoods Cliffs, NJ, 1987.
- Cline, M. W., R. A. Snay, and E. L. Timmerman, Regional deformation of the earth model for the Los Angeles region, California, *Tectonophys.*, 107, 279–314, 1984.
- DeRito, R. F., A. H. Lachenbruch, T. H. Moses, and R. J. Munroe, Heat flow and thermotectonic problems of the central Ventura basin, southern California, *J. Geophys. Res.*, 94, 681–699, 1989.
- Dong, D. N. and Y. Bock, Global Positioning System network analysis with phase ambiguity resolution applied to crustal deformation studies in California, *J. Geophys. Res.*, 94, 249–276, 1989.
- Donnellan, A., B. H. Hager, and R. W. King, Discrepancy between geologic and geodetic deformation rates in the Ventura basin, *Nature*, revised, 1993.

Donnellan, A., *A geodetic study of crustal deformation in the Ventura basin region, southern California*, PhD thesis, Calif. Inst. of Technol., Pasadena, Calif., 1991.

Drew, A. R. and R. A. Snay, Dynap-software for estimating crustal deformation from geodetic data, *Tectonophys.*, 162, 331-343, 1989.

Eberhart-Phillips, D., M. Lisowski, and M. D. Zoback, Crustal strain near the big bend of the San Andreas fault: Analysis of the Los Padres-Tehachapi trilateration networks, California, *J. Geophys. Res.*, 95, 1139-1153, 1990.

Feigl, K., D. Agnew, Y. Bock, D. Dong, A. Donnellan, B. Hager, T. Herring, D. Jackson, T. Jordan, R. King, S. Larsen, K. Larson, M. Murray, Z-K Shen, and F. Webb, Space geodetic measurement of crustal deformation in central and southern California, 1984--1992, *J. Geophys. Res.*, in press.

Herring, T., D. Dong, and R. W. King, Sub-milliarcsecond determination of pole position using Global Positioning System data, *Geophys. Res. Lett.*, 18, 1893-1896, 1991.

Herring, T., J. Davis, and I. Shapiro, Geodesy by radio interferometry: The application of Kalman filtering to the analysis of very long baseline interferometry data, *J. Geophys. Res.*, 95, 12561-12581, 1990.

Herring, T. A., Global Kalman filter VLBI and GPS analysis program, version 3.1, Massachusetts Institute of Technology, 1993.

Humphreys, E. D. and B. H. Hager, A kinematic model for the late Cenozoic development of southern California crust and upper mantle, *J. Geophys. Res.*, 95, 19747-19762, 1990.

- Hornafius, S. J., Neogene tectonic rotation of the Santa Ynez Range, western Transverse Ranges, California, suggested by paleomagnetic investigation of the Monterey Formation, *J. Geophys. Res.*, 90, 12,503-12522, 1985.
- Huftile, G. J. and R. S. Yeats, Convergence rates across a displacement transfer zone in the Western Transverse Ranges near Ventura, California, *J. Geophys. Res.*, submitted.
- Jackson, J. and P. Molnar, Active faulting and block rotations in the western Transverse Ranges, California, *J. Geophys. Res.*, 95,22,073-22087, 1990.
- King, R. W. and Y. Bock, Documentation for the MIT GPS analysis software, Massachusetts Institute of Technology, 1993.
- Kamerling, M. J. and B.P. Luyendyk, Paleomagnetism and Neogene tectonics of the northern Channel Islands, California, *J. Geophys. Res.*, 90, 12,485-12,502, 1985.
- Larsen, S. C., D. C. Agnew, and B. H. Hager, Strain accumulation in the Santa Barbara Channel: 1970-1988, *J. Geophys. Res.*, 98,2119-2133, 1993.
- Larson, K. M and F. H. Webb, Deformation in the Santa Barbara Channel from GPS measurements 1987-1991, *Geophys. Res. Lett.*, 19, 1491-1494, 1992.
- Levi, S., D. L. Schults, R. S. Yeats, L. T. Stitt, and A. M. Sarna-Wojcicki, Magnetostratigraphy and paleomagnetism of the Saugus Formation near Castaic, Los Angeles, California, in *Neotectonics and Faulting in Southern California*, pp. 103-108. Geological Society of America, 82ⁿd Annual Meeting, Guidebook and Volume, 1986.
- Luyendyk, B. P. and J. S. Hornafius, Neogene crustal rotations, fault slip, and basin development in southern California, in *Cenozoic Basin Development of Coastal California*, edited

by R. V. Ingersoll and W. G. Ernst, vol. 6, pp. 259-283. Prentice Hall, Inc., Englewoods Cliffs, NJ, 1987.

Molnar, P., Final report to the Southern California Earthquake Center for work performed during the period from September through December, 1991, technical report, Southern California Earthquake Center, Univ. Southern California, Los Angeles, 1993.

Namson, J. and T. Davis, Structural transect of the western Transverse Ranges, California Implications for lithospheric kinematics and seismic risk evaluation, *Geology*, 16,675-679, 1988.

Norris, R. M. and R. W. Webb, *Geology of California*, John Wiley & Sons, Inc., New York, 2nd edition, 1990,

Reed, R.D. and J. S. Hollister, *Structural Evolution of Southern California*, Am. Assoc. Petrol. Geol., 157 pp., 1936.

Roberts, C. W., R. C. Jachens, and H. W. Oliver, Preliminary isostatic residual gravity map of California, Open-file rep. OFR-81-573, U. S. Geol. Surv., 1981.

Rockwell, T., Neotectonics of the San Cayetano fault, Transverse Ranges, California, *Geol. Sot. Am. Bull.*, 100,850-858, 1988.

Schaffrin, B. and Y. Bock, A unified scheme for processing GPS phase observations, *Bull. Géod.*, 62, 142-160, 1988.

Stein, R. S. and R. S. Yeats, Hidden earthquakes, *Sci. Am*, June, 48-57, 1989.

Ward, S. N., North American-Pacific plate boundary, and elastic megashear, evidence from very long baseline interferometry, *J. Geophys. Res.*, 99, 7716-7728, 1988.

Webb, F. H., *Geodetic Measurement of Deformation in the Offshore of Southern California*,

PhD thesis, Calif. Inst. of Technol., Pasadena, Calif., 211 pp., 1991.

Yeats, R. S., Large-scale Quaternary detachments in the Ventura basin, southern California,

J. Geophys. Res., 88, 569-583, 1983.

Yeats, R. S. and G. J. Huftile, Alternate model for convergence across the Ventura basin,

California, *Eos, Trans. Am. Geophys. Union Supplement*, 73,590, 1992.

TABLES

Table 1: History of site occupations in the Ventura basin network. The letters refer to sub-experiments, and the x's indicate that the site was occupied for the entire experiment. Locations and **stampings** of the monuments can be found in *Feigl et al.* [1993].

Table 2: Velocities of sites relative to Santa Paula (SNPA). Units are mm and the errors represent 1σ .

Table 3: Strain calculations from GPS measurements for several regions of the network. *e* – east, *n* – north, \dot{u}_{xx} – components of velocity gradient tensor in $\mu\text{strain/yr}$, *A* – areal dilatation rate in $\mu\text{strain/yr}$, $\dot{\omega}$ – clockwise rotation rate in $^{\circ}/\text{Myr}$, $\dot{\gamma}_{1,2}$ – first and second components of horizontal shear rate in $\mu\text{rad/yr}$, $\dot{\gamma}$ – maximum horizontal shear rate in $\mu\text{rad/yr}$, θ – azimuth of maximum contraction in degrees.

Table 4: Strain calculations from triangulation data and the one epoch of GPS data, where available, for subregions of the network. $\dot{\gamma}_{1,2}$ – first and second components of **horizontal** shear rate, $\dot{\gamma}$ – maximum horizontal shear rate, θ – azimuth of maximum contraction, σ_{GPS} – wrms scatter of the triangulation angles relative to the strain rates estimated from GPS observations only, σ_{tri} – wrms scatter of angles relative to triangulation strain calculations, Δt – number of years between the first and last observed angle,

FIGURES

Figure 1: Major features of the Ventura basin region. The basin is marked by the hachured region. Locations of GPS sites in the Ventura basin network are marked by triangles. Cities and towns are marked by filled circles. Heavy lines denote faults. Dotted lines represent Quaternary **anticlinal** fold axes [*Stein and Yeats*, 1989].

Figure 2: Cross-section through the east-central portion of the Ventura basin [from *Yeats*, 1983].

Figure 3: Velocities of sites relative to Santa Paula (SNPA), which is marked by the black triangle. The error ellipses represent 95% confidence (2.450).

Figure 4: North and east baseline component versus time plots for stations with respect to PVER. The line is the position as a function of time estimated by **GLOBK**. The velocity, v , and the weighted rms scatter about the line, **wrms**, are noted in each plot. The uncertainties in the estimated horizontal velocities are all ~ 1 mm/yr (see Table 2).

Figure 5: Principal **compressional** and extensional strain-rate axes for the Ventura basin region from this study and nearby studies. The cross marks on the axes represent the standard error, 1σ , of the strain component measured from the outside of the axis. Dotted cross marks also represent the error but indicate unresolvable strain rates. (e.g., the **east-west** trending extensional component for the eastern basin). In the cases where no error bar is apparent, the size of the error is equivalent to the magnitude of the strain. The subregions used in the calculations of the strain rates are shaded. Results from other studies are marked: *L-Larsen et al. [1993]*, *E-P-Eberhart-Phillips et al., [1990]*.

Figure 6: Measured and estimated angles for the east-central (a), eastern (b), and southern (c) regions. The solid line represents the estimated rate of change from triangulation and the initial-epoch GPS measurements. The dashed line represents the rate estimated from multiple-epoch GPS measurements.

Figure 7: Residual velocities, after removal of the *Eberhart-Phillips et al. [1990]* model for slip on the San **Andreas** fault system, for sites relative to Santa Paula (SNPA), which is marked by the black triangle. The error ellipses represent 95% confidence.

	Dec	Jan	Ott	Mar	Mar	Apr	Jun	Feb	Apr	May
	86	87	87	88	89	89	90	91	91	92
CATO			A			X	C			x
COTR	X	x					A			
HAPY			B				B			x
HOPP			B			X	B			x
LACU	X	x		x	x		A	X		x
LOVE			A				c			x
MPNS							AC			x
MUNS						X 1 3				x
PVER		x	x	X	x	x	x	x	x	x
SAFE			A			x	c			x
SCLA			A				c			
SNP2			A				B			x
SNPA	X					x	x		X	X
SOLI		x					A	X		x
YAM2						X	A			x

Table 1: Site occupations in the Ventura basin network.

Site	East	North	Length
CATO	-2.1 ± 0.9	2.1 ± 0.7	-2.9 ± 0.8
COTR	-1.8 ± 1.5	6.8 ± 1.0	-5.3 ± 1.2
HAPY	2.3 ± 1.3	2.6 ± 1.0	1.9 ± 1.36
HOPP	4.5 ± 0.9	-3.4 ± 0.7	108 ± 0.9
LACU	-2.8 ± 0.8	3.0 ± 0.6	3.2 ± 0.8
LOVE	2.3 ± 1.2	-5.2 ± 1.0	$0.2^* 1.1$
MPNS	4.8 ± 1.4	-7.1 ± 1.3	-7.1 ± 1.4
MUNS	-0.8 ± 0.9	-2.0 ± 0.7	-0.9 ± 0.9
PVER	-2.0 ± 0.7	3.0 ± 0.4	-3.4 ± 0.5
SAFE	1.0 ± 0.9	-1.5 ± 0.7	1.3 ± 0.9
SCLA	0.7 ± 2.8	1.6 ± 1.9	-0.9 ± 2.1
SNP2	2.9 ± 103	-3.9 ± 1.0	-5.9 ± 2.0
SOLI	-2.3 ± 1.0	1.0 ± 0.7	1.8 ± 1.0
YAM2	-0.7 ± 2.4	$1.5^* 1.4$	1.7 ± 2.0

Table 2: Velocities relative to SNPA

	far- west	north- west	cent ral	east- cent ral	east	south
\dot{u}_{ee}	$.04 \pm .02$	$.16 \pm .03$	$.09 \pm .03$	$.10 \pm .08$	$-.10 \pm .04$	$.01 \pm .02$
\dot{u}_{en}	$.03 \pm .02$	$.02 \pm .05$	$.07 \pm .06$	$.17 \pm .08$	$.10 * .05$	$.12 * .02$
\dot{u}_{ne}	$-.09 \pm .01$	$-.13 \pm .03$	$.03 \pm .02$	$.15 \pm .06$	$-.13 \pm .03$	$-.12 \pm .02$
\dot{u}_{nn}	$-.01 \pm .02$	$-.07 \pm .04$	$-.29 \pm .04$	$-.45 \pm .06$	$-.36 \pm .04$	$-.06 \pm .02$
A	$.02 \pm .02$	$.09 \pm .05$	$-.2 \pm .05$	$-.35 \pm .10$	$-.46 \pm .06$	$-.05 \pm .03$
w	4 ± 1	4 ± 2	1 ± 2	1 ± 3	6 ± 2	7 ± 1
$\dot{\gamma}_1$	$.05 \pm .02$	$.22 \pm .05$	$.38 \pm .05$	$.55 \pm .10$	$.27 \pm .06$	$.06 \pm .03$
$\dot{\gamma}_2$	$-.06 \pm .03$	$-.10 \pm .06$	$.10 \pm .06$	$.32 \pm .10$	$-.03 \pm .06$	$.00 \pm .03$
$\dot{\gamma}$	$.08 \pm .02$	$.25 \pm .05$	$.40 \pm .05$	$.63 \pm .10$	$.27 \pm .06$	$.06 \pm .03$
e	24& 18	12* 13	-7 ± 9	-15 ± 9	3 ± 13	-2 ± 22

Table 3: Deformation parameters calculated from the GPS results

Parameter	(units)	east-central	east	south
$\dot{\gamma}_1$	($\mu\text{rad/yr}$)	$.44 \pm .26$	$.31 \pm .06$	$.02 \pm .06$
$\dot{\gamma}_2$	($\mu\text{rad/yr}$)	$-.07 \pm .10$	$.08 \pm .05$	$-.04 \pm .08$
$\dot{\gamma}$	($\mu\text{rad/yr}$)	$.45 \pm .26$	$.33 \pm .06$	$.04 \pm .08$
θ	(deg)	4 ± 13	-7 ± 8	31 ± 61
σ_{GPS}	arcseconds	1.6	1.0	0.9
σ_{tri}	arcseconds	1.1	0.9	0.9
n_{obs}		15	48	28
Δt	years	28	58	77

Table 4: Strain calculations from triangulation

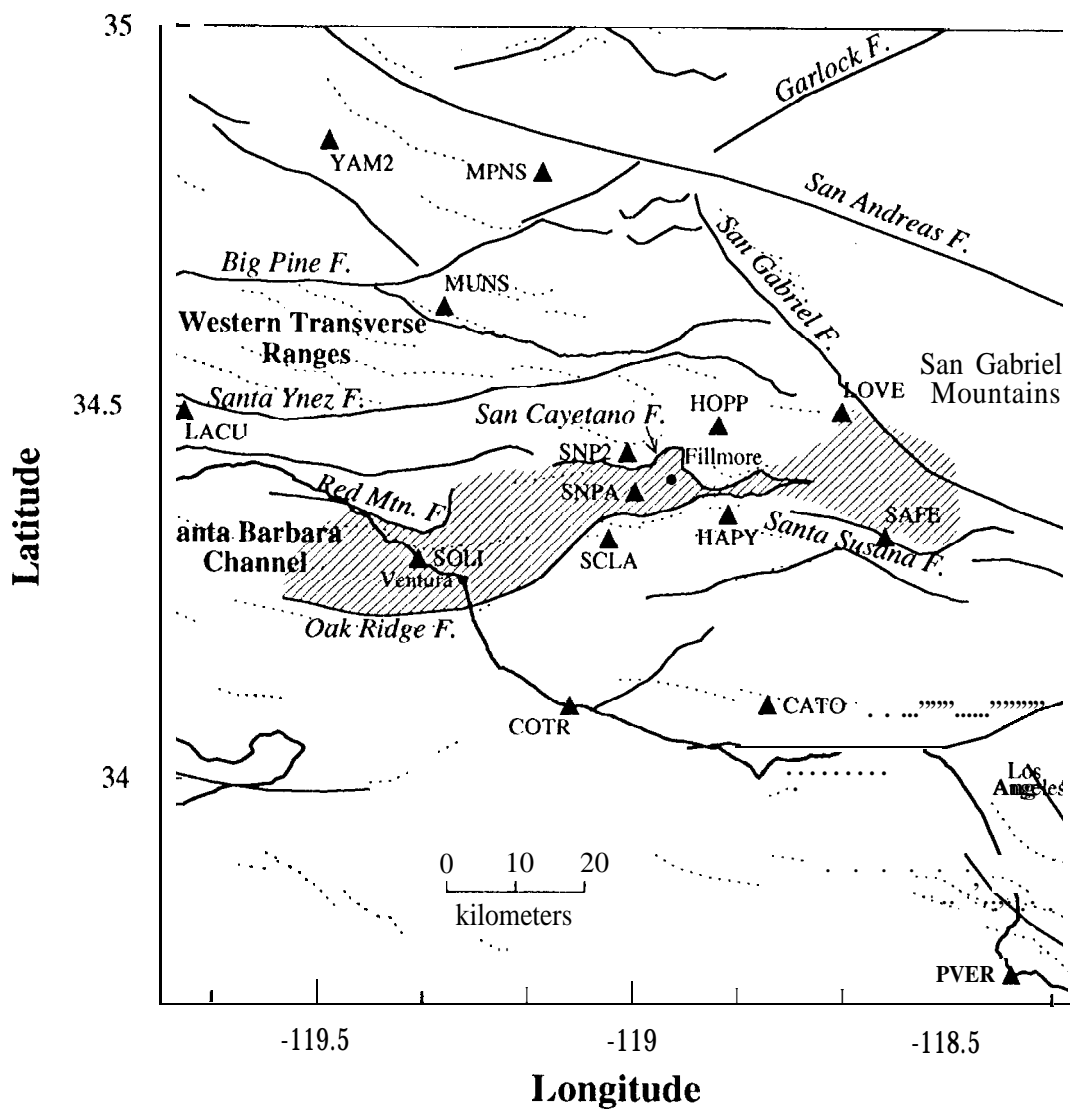


Figure 1

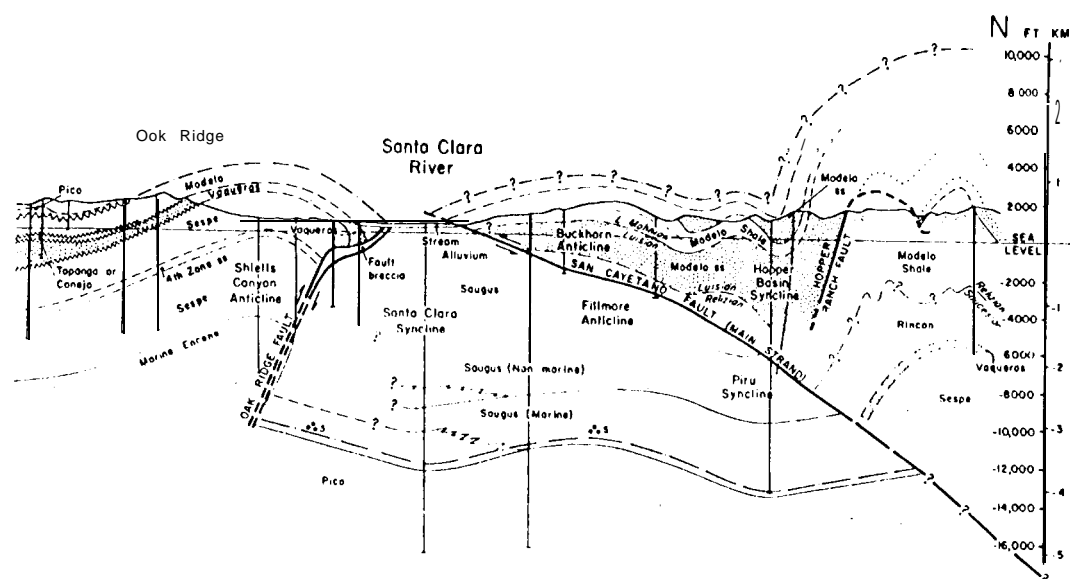
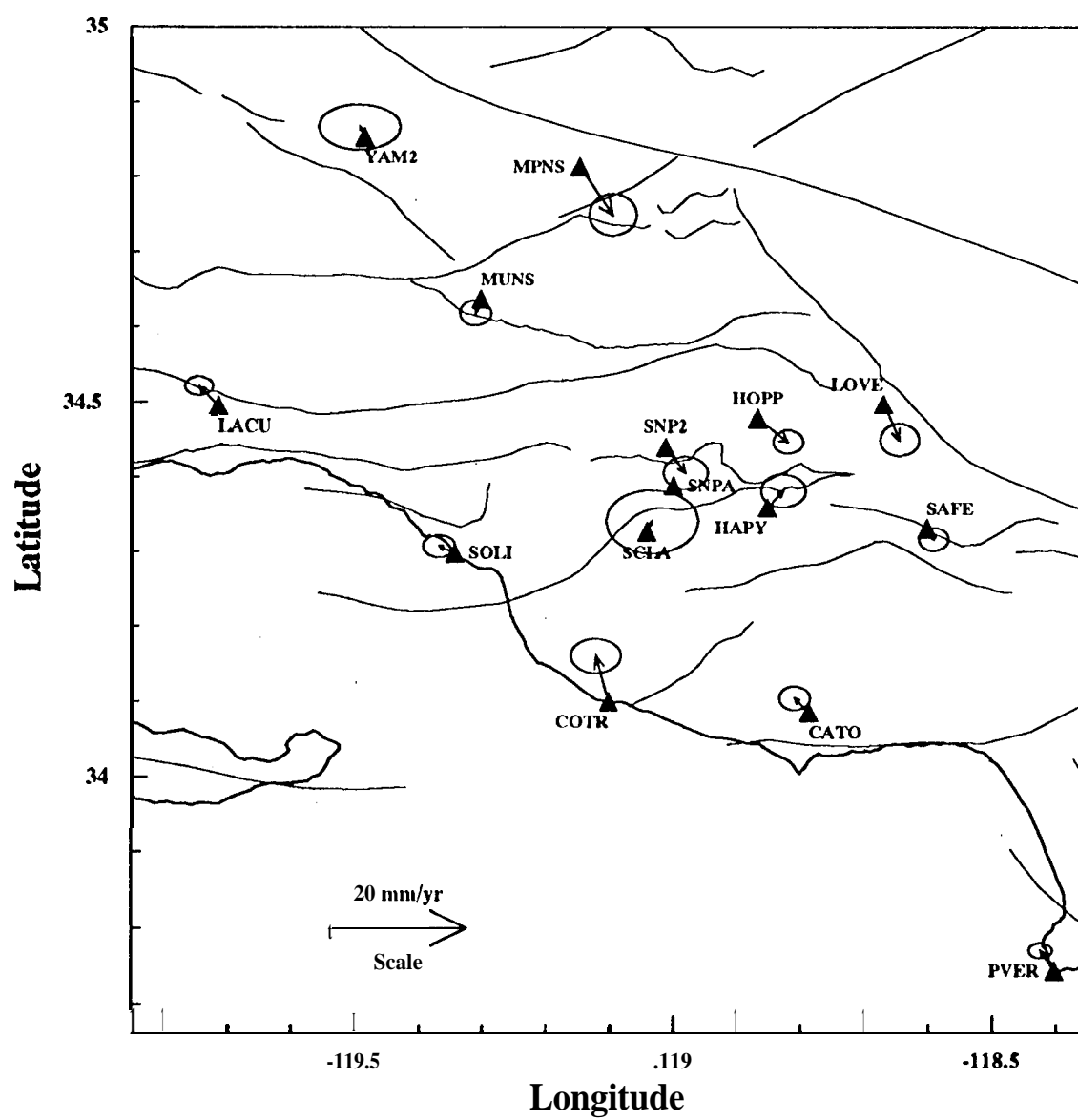


Figure 2



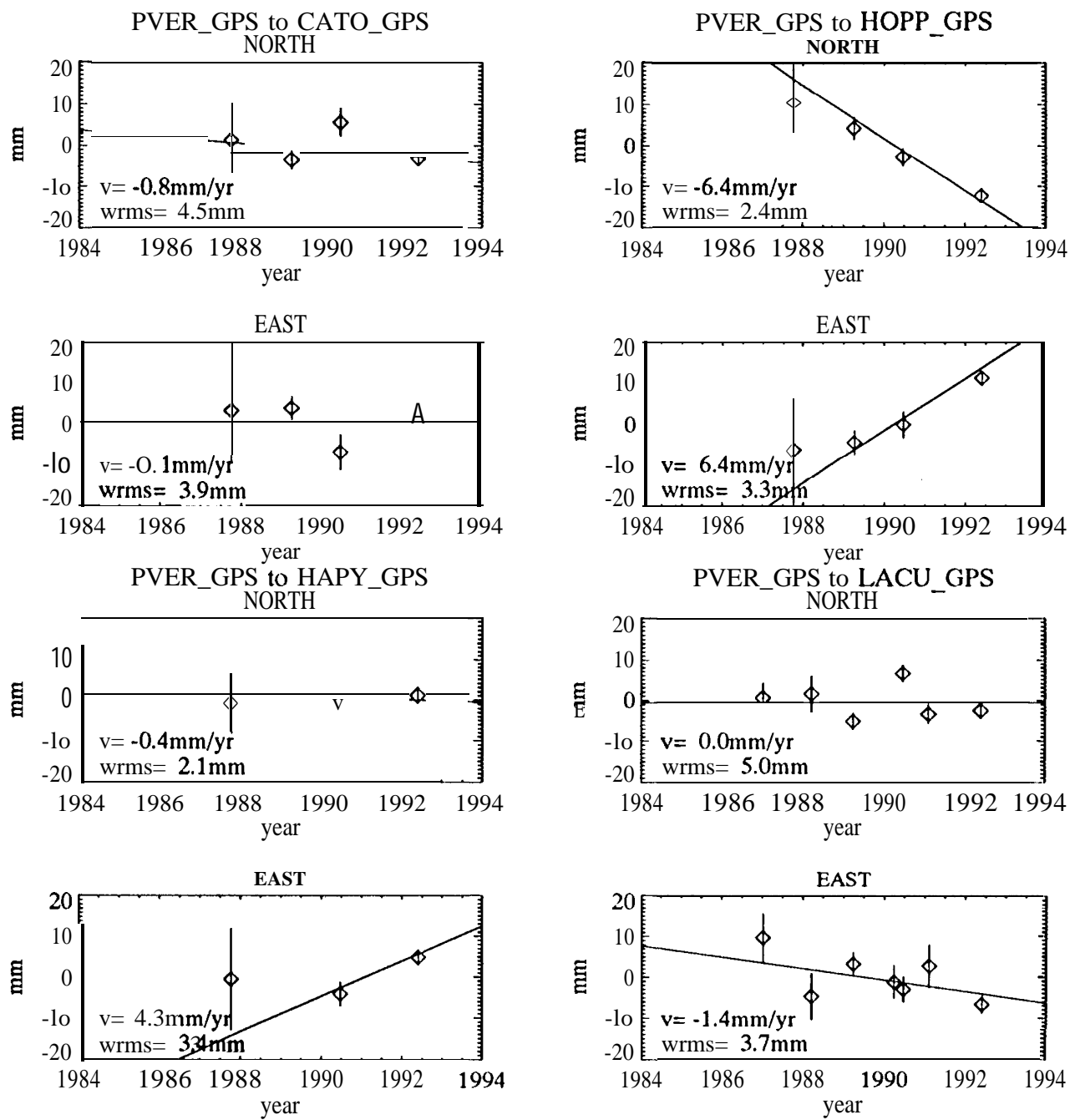


Figure 4

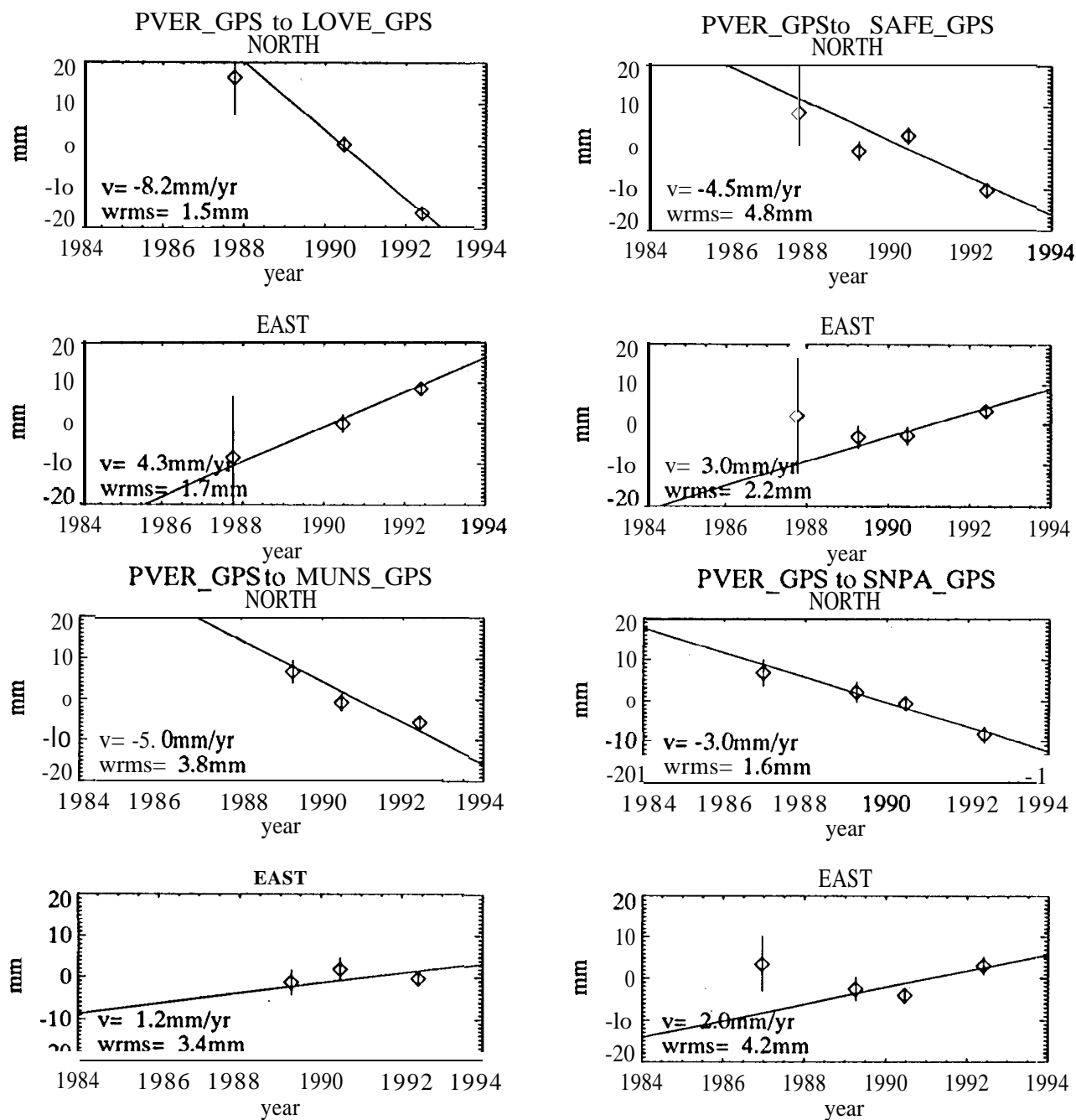


Figure 4 (cont.)

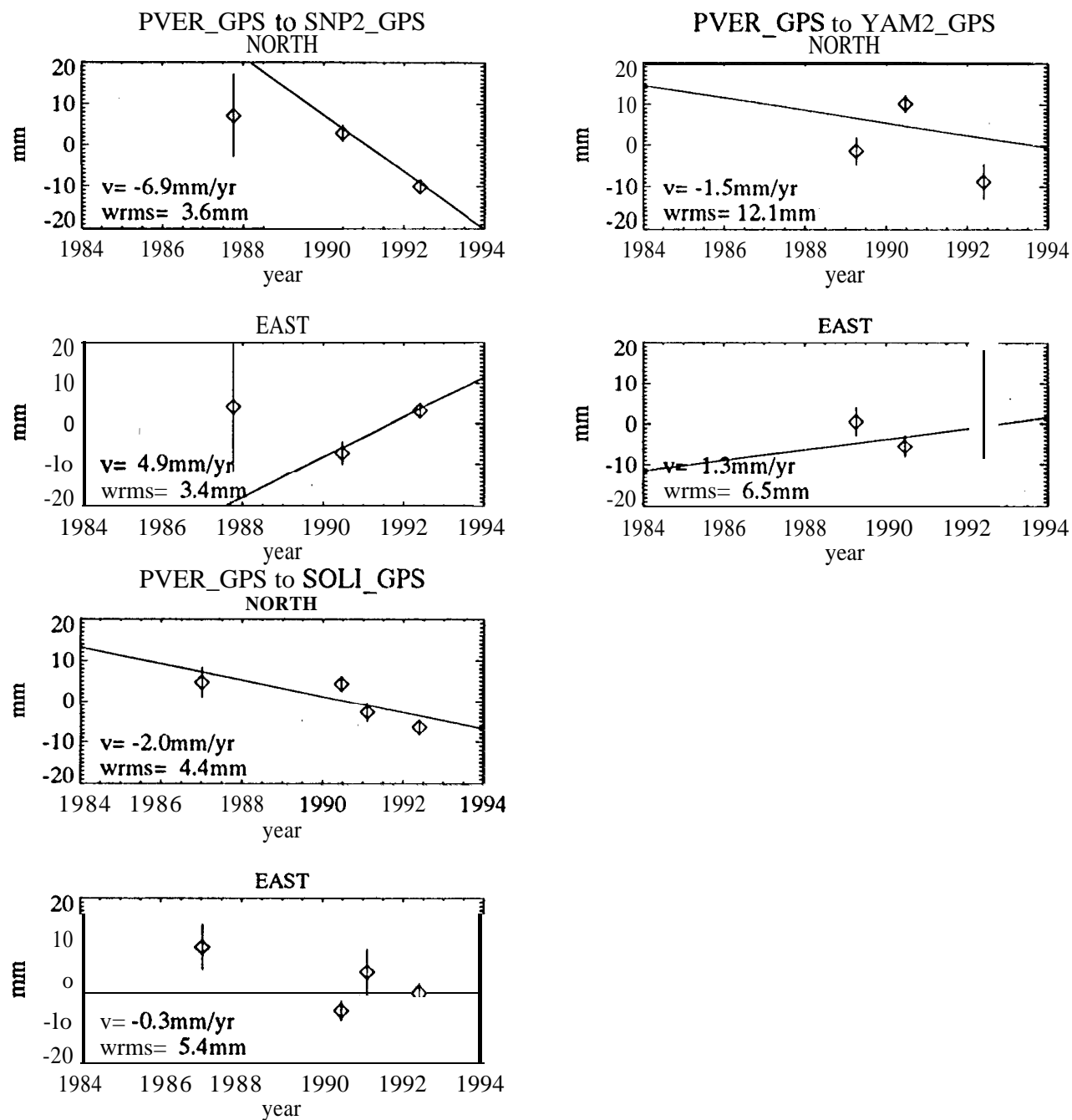


Figure 4 (cont.)

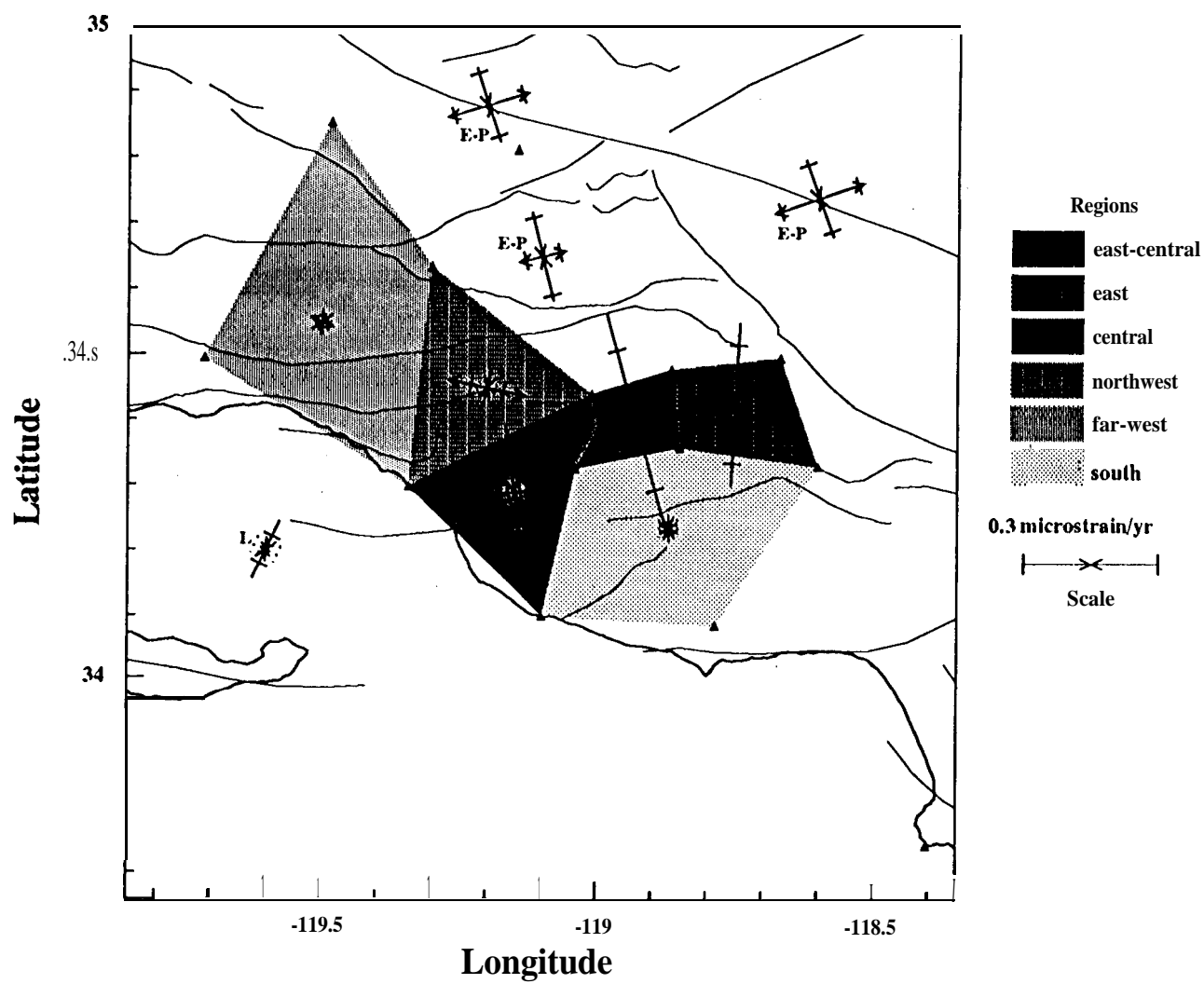


Figure 5

East-Central Basin

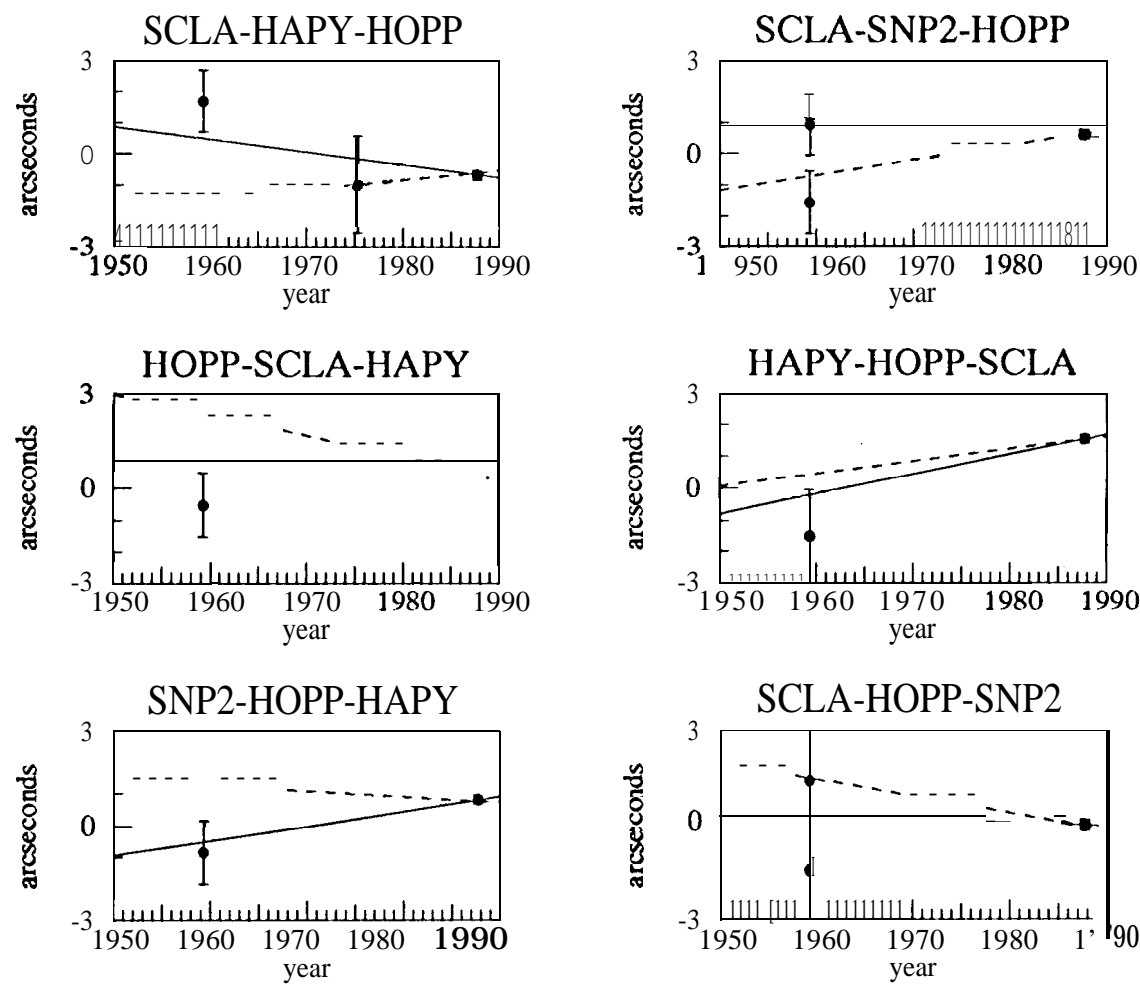


Figure 6a

Eastern Basin

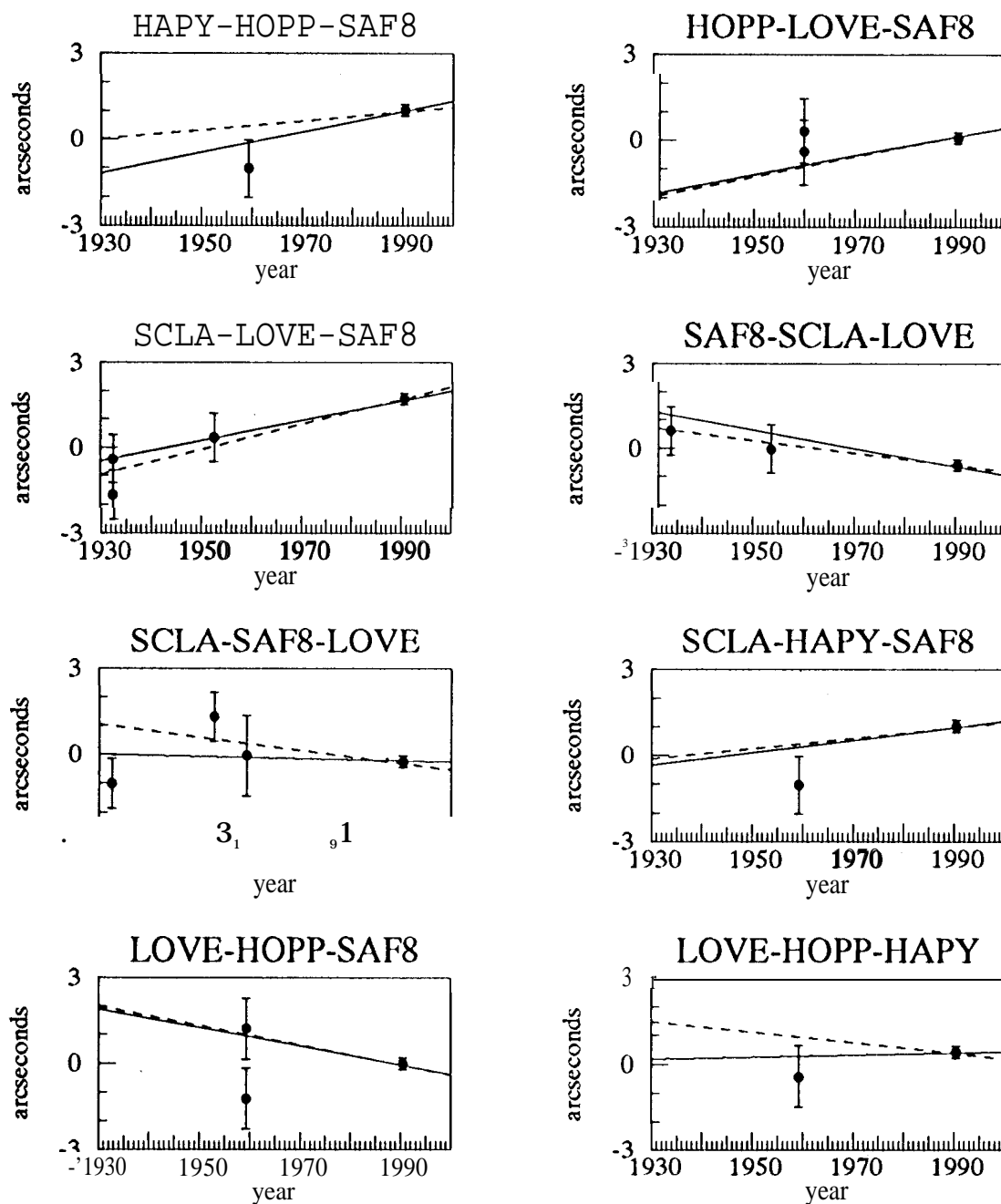


Figure 6b

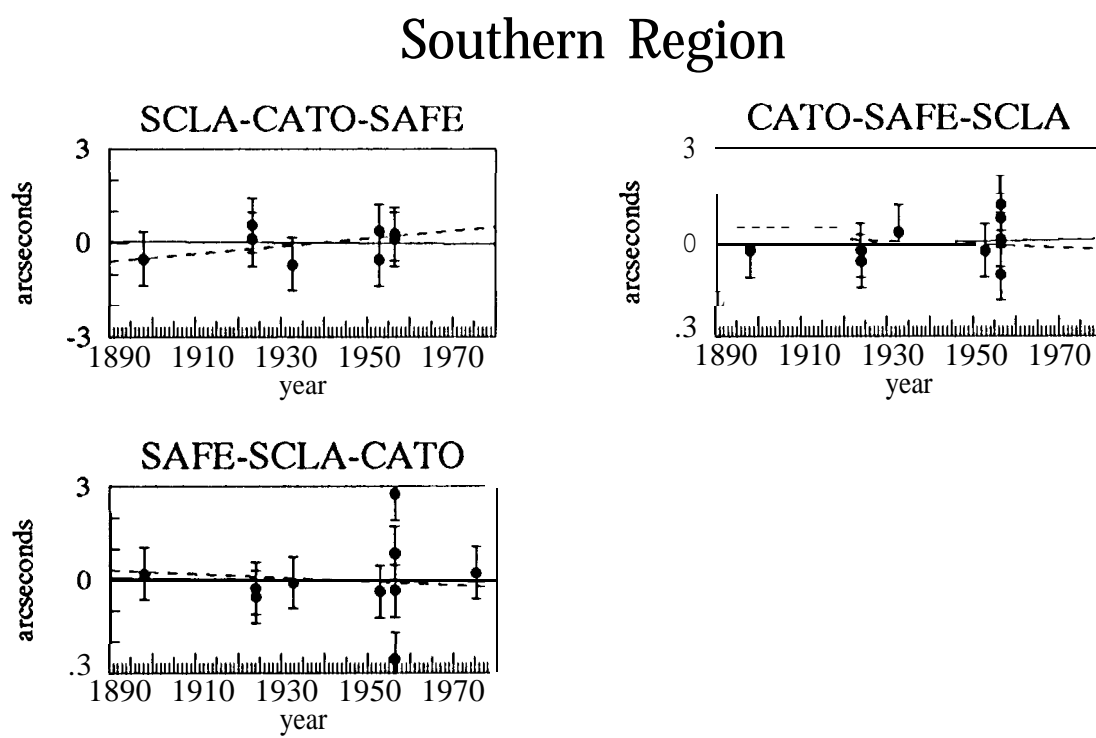


Figure 6c

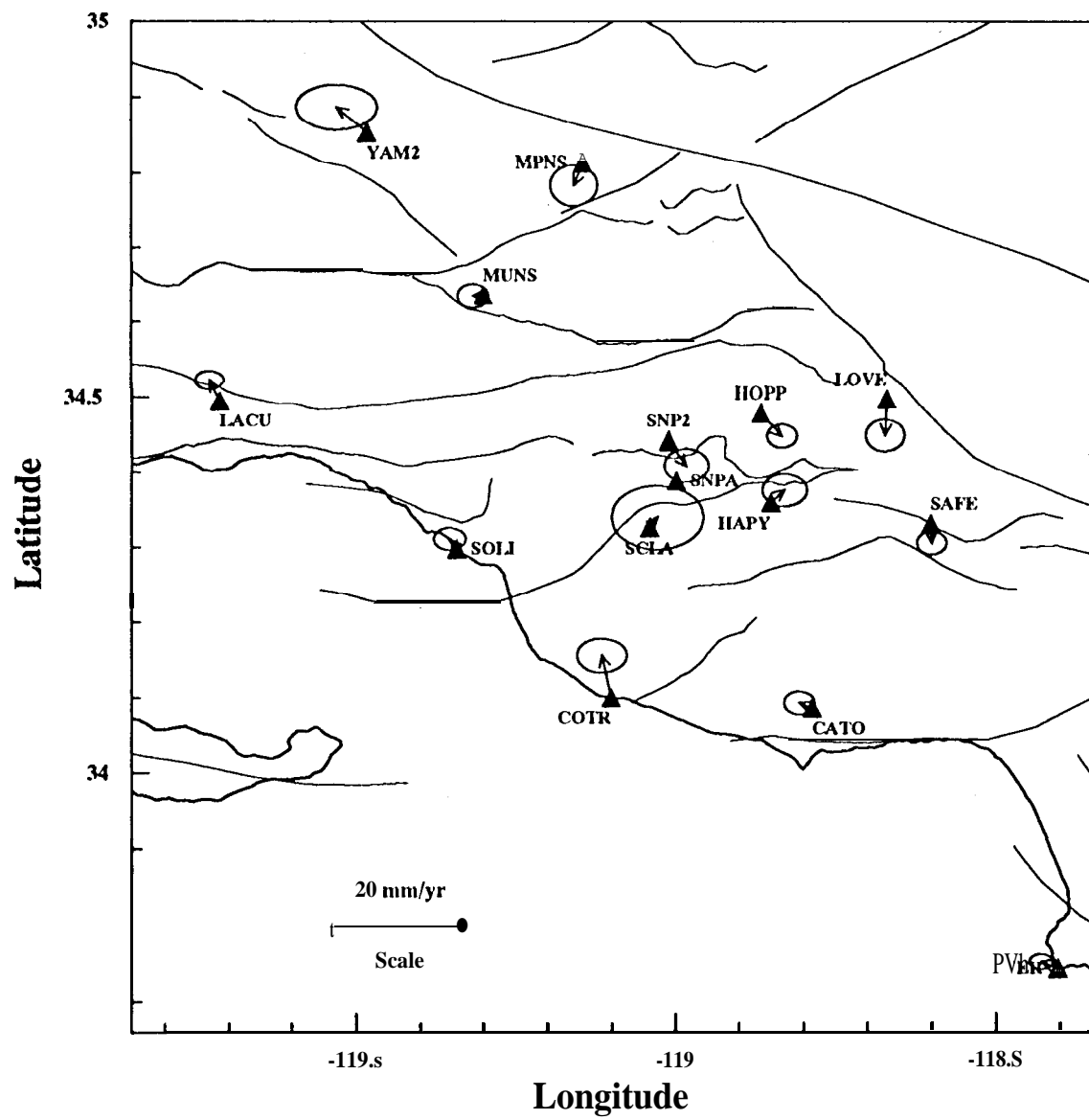


Figure 7